ELSEVIER

Catalysis Today 78 (2003) 419–432

CATALYSIS TODAY

www.elsevier.com/locate/cattod

Abatement of volatile organic compounds: oxidation of ethanal over niobium oxide-supported palladium-based catalysts

Roberta Brayner [a], David dos Santos Cunha [b], François Bozon-Verduraz [a,*]

[a] *LCMDC, ITODYS, CNRS UPRES-A 7086, Université Paris 7 Denis Diderot, case 7090, 2 Place Jussieu, 75251 Paris Cedex 05, France*

[b] *Laboratório de Combustão e Propulsão, INPE, Rodovia Presidente Dutra, Km 40, Cachoeira Paulista 12630-000 SP, Brazil*

Abstract

Niobium-supported palladium-based catalysts (Pd, Pd–Cu and Pd–Au) were employed in the oxidation of ethanal. The catalysts were prepared according to original methods by either *multi-steps* (anchoring of complexes, calcination and reduction) or *one-step* (photoassisted reduction) procedures. The oxidation of ethanal was carried out in gas phase in a dynamic-differential reactor at 300 °C at atmospheric pressure. The activity/selectivity of the catalysts depend on (i) the catalyst preparation; (ii) the presence of a second metal. Addition of Au or Cu decreases the catalysts deactivation and the best performance in total oxidation was obtained with Pd–Au/Nb_2O_5 prepared by photoassisted reduction. As shown by in situ IR spectroscopy of adsorbed CO, this peculiarity may be ascribed to Au → Pd electron donation, which prevents the surface oxidation of palladium particles.

Keywords: Pd–Cu; Pd–Au; Nb_2O_5; Oxidation; Ethanal; CO_2; Photoreduction; IR spectroscopy of adsorbed CO

1. Introduction

Over the last decade, niobium pentoxide has attracted an increased interest in catalysis as support, additive or active phase [1] and recent works have invoked electronic effects in niobia-supported hydrogenation catalysts [2,3]. However, little attention has been paid to: (i) the influence of the catalysts preparation method; (ii) the redox and semiconducting character of Nb_2O_5 [4]; and (iii) its use in oxidation reactions. *Volatile organic compounds* (VOC) have long been a major source of air pollution [5]. They arise from a variety of industrial and commercial processes including printing, metal cleaning and decoration, paint drying, manufacturing of organic compounds and polymers, food processing.

The conversion of oxygenates show particular difficulties. In addition, the use of ethanol in fuels (e.g. in Brazil) leads to the release of ethanal in automobile exhausts. The desired reaction is the complete oxidation of the VOC to CO_2 and H_2O. Recently, the catalytic oxidations of H_2, CO, ethanal and cyclohexene over heteropolycompounds (alkali salts of 12-molybdophosphoric acid) were correlated with the reducibility of catalysts by CO [6].

The present work concerns the oxidation of acetaldehyde over niobia-supported palladium-based metallic catalysts (Pd, Pd–Cu and Pd–Au); it involves preparation procedures such as photodeposition and grafting, original on niobia. The aim of this work is to correlate the preparation methods and the second

* Corresponding author. Fax: +33-1-44-27-61-37.
E-mail address: bozonver@ccr.jussieu.fr (F. Bozon-Verduraz).

0920-5861/02/$ – see front matter © 2002 Elsevier Science B.V. All rights reserved.
PII: S0920-5861(02)00321-8

metal addition with the activity/selectivity to CO_2 production in gas phase ethanal oxidation.

2. Experimental

Nb_2O_5-HY-340 was kindly supplied by CBMM, Brazil, $Pd(NO_3)_2$, $HAuCl_4$ and $KAu(CN)_2$ were obtained with the courtesy of Engelhard, CLAL, France.

2.1. Preparation methods

2.1.1. Anchoring (Pd/Nb_2O_5 and $Pd–Cu/Nb_2O_5$)

Pd and Cu acetylacetonates were anchored on niobia from their solution in toluene at a fixed temperature in the 60–80 °C range [7]. The solid obtained after filtering and washing by toluene at room temperature (RT) was calcined at 400 °C for 12 h under flowing oxygen. The reduction was achieved by a 10% H_2/He mixture at 200 °C for Pd/Nb_2O_5 and 400 °C for $Pd–Cu/Nb_2O_5$.

2.1.2. Photoassisted reduction (Pd/Nb_2O_5, $Pd–Cu/Nb_2O_5$ and $Pd–Au/Nb_2O_5$)

The photoassisted reduction occurs when a semiconducting support is illuminated with photons of energy $E > E_g$ (band gap width: 3.4 eV for Nb_2O_5) in the presence of the metal precursor in solution. The reduction of the metal ions $[Pd(H_2O)_4]^{2+}$, $[Cu(H_2O)_4]^{2+}$ and $Au(CN)_2^-$ aqueous solution is achieved by the electrons produced by the support under illumination provided that the associated holes are rapidly consumed by a *hole scavenger*, such as propane-2-ol in the reaction medium [8–11]. Nb_2O_5 was dipped into a 1/1 mixture of propane-2-ol and H_2O; the precursor was then added and the suspension was continuously stirred during irradiation with a high-pressure mercury lamp. The solids obtained after filtering and washing by propane-2-ol at RT were dried at 60 °C overnight.

2.2. Techniques

Chemical analyses were carried out at the Materials Engineering Department, DEMAR/FAENQUIL, Lorena, SP, Brazil by inductively coupling plasma atomic emission spectroscopy (ICP-AES).

X-ray powder diffraction (XRD) patterns were recorded using Co Kα radiation. The diffractometer was calibrated using a standard Si sample. The counting time was 30 s per step (2θ) of 0.05°. The mean crystallite size was estimated using the *Scherrer* equation, after computer fitting using a *pseudo-Voigt* function (software Profile, SOCABIM Diffract, At).

TEM measurements were performed with a JEOL 100 CXII microscope operating at 100 kV. The particle size distribution was obtained from the TEM pictures using a digital camera and the SAISAM and TAMIS software (Microvision Instruments), calculating the surface-average particle diameter from $d_P = \sum n_i d_i^2 / \sum n_i d_i$.

X-ray energy dispersive spectrometry (EDX) was carried out with a LINK AN 10000 system (Si-Li detector) connected to a JEOL JEM CXII transmission electron microscope operating at 100 kV and equipped with an ASID 4D scanning device (STEM mode). The X-rays emitted from the specimen upon electron impact were collected in the 0–20 keV range for 200–400 s. Atomic compositions (%) were obtained with the 2LINK program (RTS-2/FLS).

Transmission infrared spectra were recorded in the 2200–1800 cm^{-1} range using an Equinox 55 Bruker FT-IR spectrometer equipped with a DTGS detector. The samples were pressed into self-supporting discs (about 10 mg cm^{-2}) and placed in a stainless steel cell (In Situ Research Instruments) allowing in situ analysis of samples in the 20–500 °C range, including CO adsorption. The spectra were recorded by averaging 1000 scans (with a scanning velocity of 6.25 Hz and a spectral resolution of 4 cm^{-1}) and smoothed through the *Savitzky–Golay* algorithm with a smoothing degree of 13.

UV-Vis-NIR diffuse reflectance spectra (DRS) were recorded on a Cary 5E spectrophotometer equipped with a PTFE-coated integration sphere.

Hydrogen chemisorption was carried out at the National Institute of Spatial Research (INPE, Cachoeira Paulista, SP, Brazil). Samples were evacuated (10^{-5} Torr) while the temperature was raised slowly from RT to 70 °C, then treated with 250 Torr H_2 (1 Torr = 133.3 Pa) at 70 °C (1st isotherm), evacuated again (10^{-5} Torr) and then treated with 250 Torr of H_2 at 70 °C (2nd isotherm). The H/Pd data obtained were considered as the metal fraction exposed (MFE).

Oxidation of ethanal was carried out at 300 °C in a conventional flow quartz reactor (total flow rate ranged between 70 and 100 $cm^3\,min^{-1}$) with a mixture of 10% O_2/N_2. The reaction products (CO_2, ethanol, acetone, methanal, crotonaldehyde, ethyl acetate and acetic acid) were analyzed by gas chromatography using a Porapak Q column.

3. Results and discussion

Table 1 collects the characteristics of the samples prepared and tested in ethanal oxidation.

3.1. Characterization of Pd/Nb_2O_5 samples

TEM micrographs of the monometallic anchored catalyst A-PD1 (not presented) show a statistical repartition of the particles with a mono-modal particle size distribution (average size $d_P \approx 2.7$ nm; Table 1); the MFE measured by H_2 chemisorption was about 70% (Table 1). For the samples prepared by photoreduction, the particle size distribution is heterogeneous, with a higher value of the average particle size (4–6 nm) and a lower MFE (near 45%, Table 1); it was also observed that the particles agglomeration begins to be important when the metal content is higher than 5 wt.%.

The interaction of $Pd(acac)_2$ with niobia was studied by UV-Vis-NIR DRS. The DR spectrum of pure Nb_2O_5 calcined at 400 °C (Fig. 1, spectrum 'a') is characterized by a strong absorption in the UV range due to the interband transition and allows the estimation of the band gap width (3.4 eV, absorption threshold near 360 nm) [7]. The DRS of the A-PD1 sample *after anchoring* (Fig. 1b) shows a shoulder near 415 nm due to d–d transition of $Pd(acac)_2$ [12]. After heating in flowing O_2 at 400 °C, the shoulder

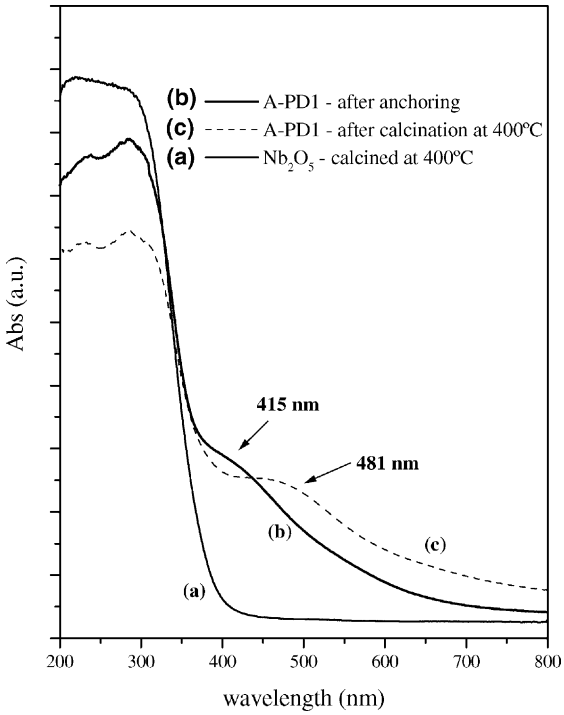

Fig. 1. DR spectra of (a) pure niobia calcined at 400 °C; (b) A-PD1 sample after anchoring; and (c) A-PD1 sample after calcination at 400 °C.

near 415 nm is shifted to 481 nm (Fig. 1c). This can be ascribed to the formation of isolated Pd^{2+} ions (or to small *palladium–oxygen* entities) and not to bulk PdO particles, whose absorption threshold lies in the NIR range (band gap width equal to 0.8 eV) [12]. These results were confirmed by XANES/EXAFS measurements [13].

After reduction, all samples were analyzed by FT-IR of adsorbed CO. Infrared studies of CO chemisorption on Pd are numerous; they have concerned

Table 1
Characteristics of the niobia-supported samples

Sample	Preparation method	Composition weight (%)	d_P (nm) TEM	S_g (m^2/g)	H/Pd[a]
A-PD1	Anchoring	1.3Pd	2.7	103	0.70
PH-PD3	Photoreduction	2.9Pd	4.0	118	0.45
A-PDCU2	Anchoring	0.7Pd0.6Cu	Pd = 4.6, Cu = 18.7	95	0.11
PH-PDCU1	Photoreduction	2.7Pd0.9Cu	5.5	100	0.25
PH-PDAU3	Photoreduction	2.7Pd0.9Au	7.6	102	0.50

[a] H adsorbed/total Pd ratio.

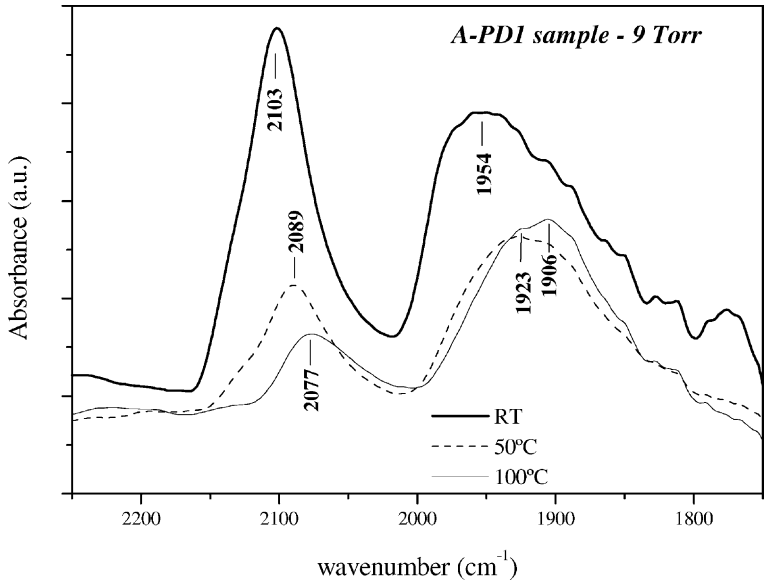

Fig. 2. A-PD1 sample: in situ IR spectra of adsorbed CO ($P = 9$ Torr) upon increasing temperature.

either palladium supported on various oxides or single crystals [12,14-21] but studies concerning the palladium/niobia system are scarce [22]. For the *anchored* sample A-PD1 (Fig. 2), adsorption at RT gives a peak at 2103 cm^{-1} which is attributed to linear (L) Pd^0–CO species in interaction with residual Pd^{n+} ionic species. The broad band recorded in the 2000–1800 cm^{-1} range is ascribed to bridged compressed (B_2), isolated (B_2) and (B_3) species [14]. The linear/bridged intensity ratio ($L/(B + L)$) amounts to about 50% (Table 2), indicating a high MFE, confirmed by H_2 chemisorption (Table 1). After adsorption at 50 and 100 °C, the band initially centered at 2103 cm^{-1} is weakened and shifted to 2077 cm^{-1}, whereas the band assigned to *bridged* CO species moves to lower wavenumbers. This tendency may be explained by the achievement of the reduction of palladium and the sintering of the Pd particles (Table 2).

Table 2
Intensity ratio of linear and bridged species at various temperatures ($P_{CO} = 3$ Torr)

Temperature (°C)	Linear (L)	Bridged (B)	Total surface	$L/(L + B)$
A-PD1				
RT	0.954	0.945	1.899	0.50
50	0.307	0.752	1.059	0.29
100	0.116	1.027	1.143	0.11
PH-PD3				
RT	1.233	5.287	6.520	0.19
50	0.683	4.528	5.211	0.13
100	0.341	5.535	5.876	0.06

On the PH-PD3 sample (prepared by *photoreduction*) (Fig. 3), CO adsorption at RT generates a shoulder at 2158 cm^{-1} (Pd^{2+} species), two intense peaks at 2135 cm^{-1} (Pd^{+} species) and 2099 cm^{-1} (*linear* Pd^0–CO in interaction with residual Pd^{n+} ionic species) with a strong broad band between 2000 and 1800 cm^{-1}. The linear/bridged ratio decreases also upon increasing the CO adsorption temperature, which is still due to Pd particle sintering (Table 2). To sum up: (i) the presence of residual Pd^{+} and Pd^{2+} species shows that the reduction is not complete, in agreement with the results obtained by photoelectron spectroscopy (XPS spectra, not shown); (ii) the linear/bridged intensity ratio, is lower than in the case of the A-PD1 sample, which indicates that the MFE is smaller, in agreement with the H_2 adsorption measurements (Table 1).

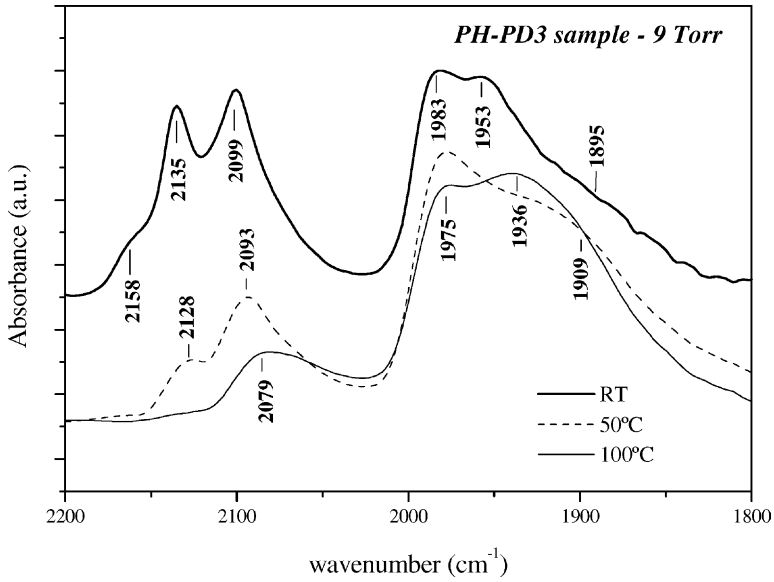

Fig. 3. PH-PD3 IR sample: in situ IR spectra of adsorbed CO ($P = 9$ Torr) upon increasing temperature.

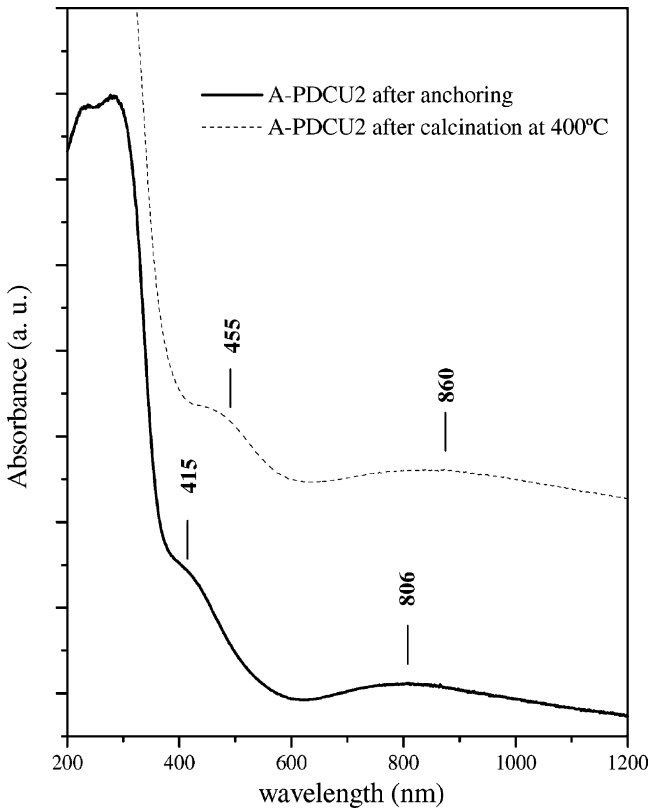

Fig. 4. DR spectra of A-PD1 sample *after anchoring* and *after calcination* at 400 °C.

3.2. Characterization of bimetallic samples

3.2.1. Pd–Cu system

The UV-Vis-NIR DR spectrum of the *anchored* sample A-PDCU2 (Fig. 4) shows a shoulder near 415 nm ascribed to d–d transitions of $Pd(acac)_2$ [12] and a broad asymmetric band centered at 806 nm due to d–d transitions of $Cu(acac)_2$ [23]. After heating in flowing O_2 at 400 °C, the shoulder and the asymmetric band are shifted to 455 and 860 nm, respectively (Fig. 4) due to the acetylacetonate ligand decomposition and its substitution by an *oxygen monodentate ligand* which generates a weaker ligand field than the acetylacetonate *bidentate ligand*. The entities involved can be identified to isolated Pd^{2+} and Cu^{2+} isolated entities and not to bulk PdO and CuO particles; the oxides indeed, are semiconducting and show interband transition, with absorption edge near 0.8 eV (1700 nm) [12] and 1.4 eV (890 nm), respectively, whereas, for the former species, transitions between levels are expected. XRD measurements after reduction confirm the presence of metallic Pd^0 and Cu^0 isolated particles without alloy formation; the mean particle size d_P (observed by TEM) are 4.6 and 18.7 nm for Pd and Cu, respectively (Table 1).

For the PH-PDCU1 sample (prepared by *photoreduction*), Pd metal was deposited first and the Cu precursor reduced on Pd particles. In this case, the Pd particles act as nuclei for the growth of Cu particles. The mean particle size d_P of the particles is 5.5 nm; EDX analysis shows that the particles contain palladium and copper in different amounts but no alloy formation is observed.

Several IR studies have been devoted to the chemisorption of CO on supported [24–30] or unsupported [29] Cu. Copper is able to form stable Cu^+–CO carbonyl species [24,25]. This stability is due to the simultaneous ligand → metal σ-donation and metal → ligand π-back-donation. The latter process results in strengthening the metal–carbon bond and is responsible for the thermal stability of many transition-metal CO complexes [24]. On the other hand, Cu^{2+}–CO species are very labile as the back donation is absent [26]. In addition, Cu^0–CO end-on species present a weak band centered at 2110 cm^{-1} very close to the Cu^+–CO band. These two species have a common absorption range of about 30 cm^{-1} [27]. The comparison between monometallic Pd and bimetallic Pd–Cu catalysts *prepared by anchoring* is presented on Fig. 5. After CO adsorption at RT, the A-PDCU2 sample presents: (i) a weak band centered at 2170 cm^{-1} attributed to Cu^{2+}–CO species; (ii) a very intense peak centered at 2142 cm^{-1} assigned to Cu^+–CO; and (iii) a very weak shoulder near 2090 cm^{-1}, which can

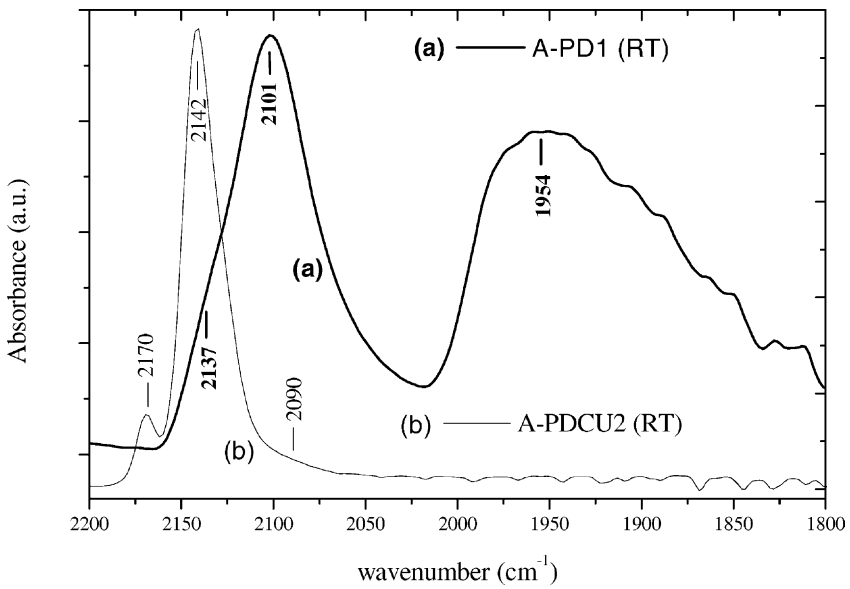

Fig. 5. IR spectra of adsorbed CO ($P_{CO} = 9$ Torr) at RT. Comparison between A-PD1 and A-PDCU2 samples.

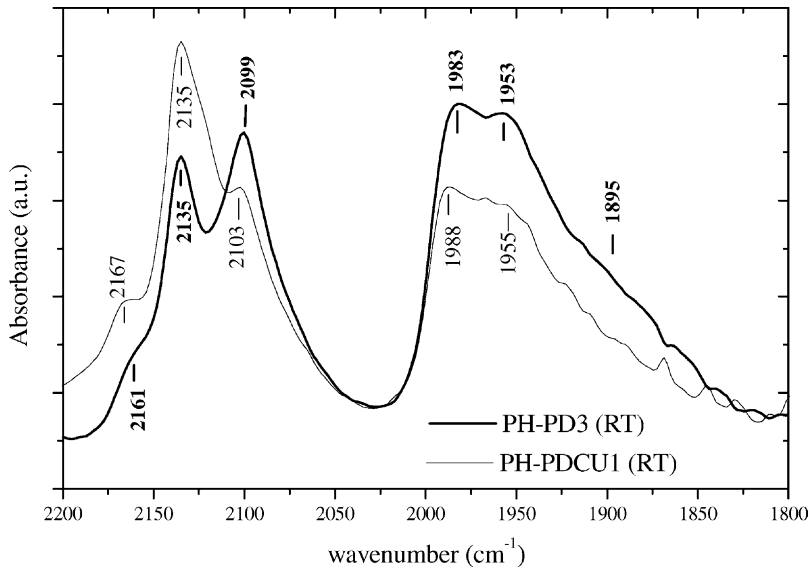

Fig. 6. IR spectra of adsorbed CO ($P_{CO} = 9$ Torr) at RT. Comparison between PH-PD3 and PH-PDCU1 samples.

be ascribed to Pd^0–CO *linear* species. Finally, no *bridged* Pd^0 species were formed upon either increasing or decreasing CO pressure. These results show that most palladium atoms are covered by copper species, which is supported by the low value of the H/Pd ratio (0.11, Table 1).

The spectra of the monometallic (PH-PD3) and bimetallic (PH-PDCU1) samples prepared by *photodeposition* (Fig. 6) do not differ significantly except for the enhancement of the peak at 2135 cm^{-1} in the latter case, which may be ascribed to the contribution of Cu^+–CO species. The presence of an intense

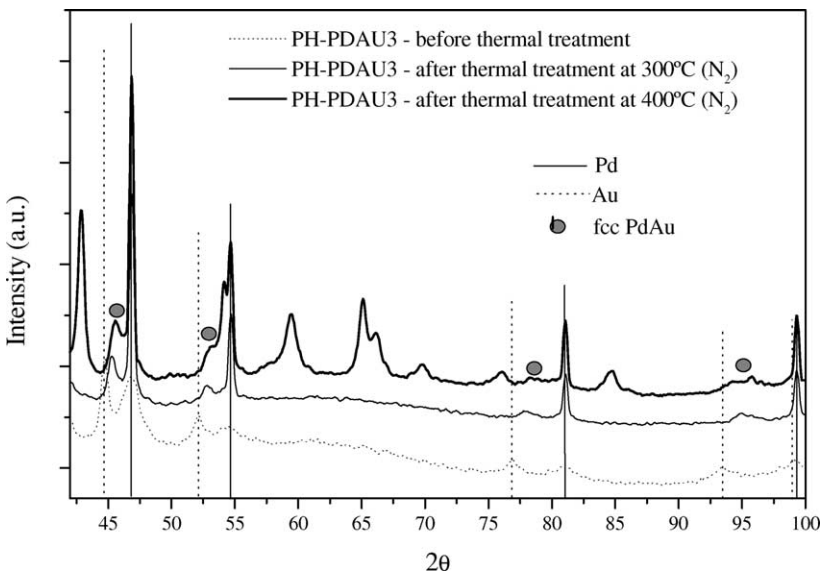

Fig. 7. X-ray diffraction pattern of the Pd–Au/Nb_2O_5 sample (PH-PDAU3).

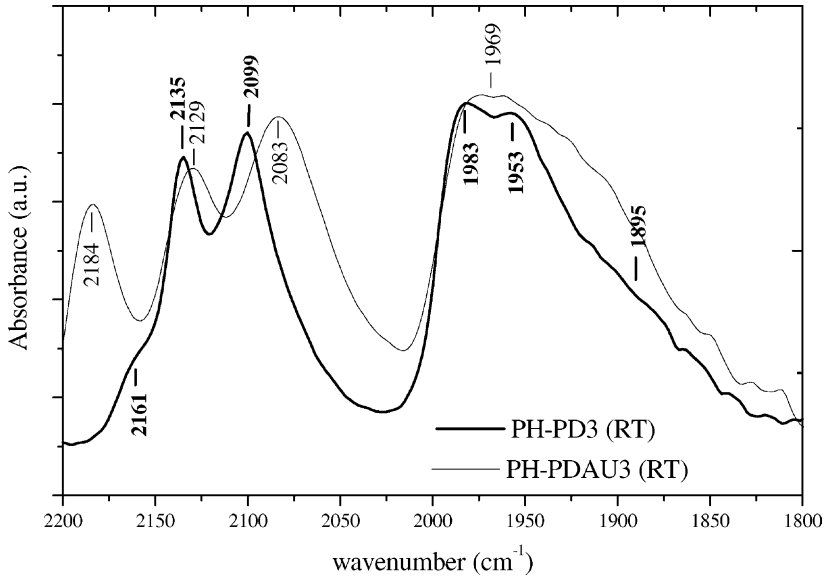

Fig. 8. IR spectra of adsorbed CO (P_{CO} = 9 Torr) at RT. Comparison between PH-PD3 and PH-PDAU3 samples.

massif peaking at 1988 and 1955 cm^{-1}, due to *compressed and isolated bridged* $(CO)_2$ Pd^0 (absent on the anchored sample), suggests that most of the copper atoms are covered by palladium atoms and ions.

3.2.2. Pd–Au system

The bimetallic Pd–Au samples were prepared only by the photoreduction method. After 1 h irradiation of the niobia suspension in $KAu(CN)_2$, the color of the medium changes from white to light red, which is due to the formation of Au^0 particles (plasmon resonance). When the yellow solution of $Pd(NO_3)_2$ is added, the color of the gold solution changes drastically from light red to dark reddish-gray. It may be inferred that the Au particles act as nuclei for the of Pd particle growth. In this case, H_2 chemisorption shows that the surface is enriched in palladium (MFE = 50%; Table 1) compared to the PH-PD3 monometallic sample (MFE = 45%). The final d_P value is 7.6 nm, whereas EDX analysis shows that the particles contain palladium and gold in different amounts. According to XRD measurements performed after irradiation, Pd^0 and Au^0 are not combined; however, after thermal treatment between 100 and 400 °C under flowing N_2, a Pd–Au (f.c.c.) alloy is formed (Fig. 7).

Fig. 8 compares the spectra of the monometallic Pd and of the bimetallic Pd–Au samples after CO adsorption at RT The latter presents (i) a peak centered at 2184 cm^{-1} attributed to Au^+–CO species; (ii) a band at 2129 cm^{-1} ascribed to Au^0–CO species;

Table 3
Oxidation of ethanal at 300 °C

Sample	Composition weight (%)	S_{CO_2} (%)[a]	S_{AcOH} (%)[a]	C_{90} (%)[a]	CO_2 production mol/s g_{Pd}[a]	AcOH production mol/s g_{Pd}[a]
A-PD1	1.3Pd	45	19.3	28.4	1.5×10^{-3}	1.2×10^{-3}
PH-PD3	2.9Pd	72	10.0	10.2	8.3×10^{-4}	7.4×10^{-4}
A-PDCU2	0.7Pd0.6Cu	43	41.0	48.9	4.3×10^{-3}	4.0×10^{-3}
PH-PDCU1	2.7Pd0.9Cu	58	20.7	19.7	9.2×10^{-4}	4.8×10^{-4}
PH-PDAU3	2.7Pd0.9Au	65	15.0	53.0	1.0×10^{-3}	3.3×10^{-4}

[a] Measured after 90 min of reaction.

(iii) a peak at 2083 cm^{-1} assigned to Pd^0–CO linear species; and finally (iv) a large massif centered at around 1969 cm^{-1} ascribed to Pd^0–CO *bridged* species. Whereas the band at 2129 cm^{-1} disappears upon outgassing at RT, the band centered at 2184 cm^{-1} is still observed after evacuation at 100 °C (spectrum not shown). This stability of the Au^+–CO species and the band shift of the Pd^0–CO *linear* species from 2101 cm^{-1} (PH-PD3 monometallic sample) to 2083 cm^{-1} (PH-PDAU3) are indicative of an *electronic effect* (Au → Pd electron donation); this is in agreement with a previous work of Kugler and

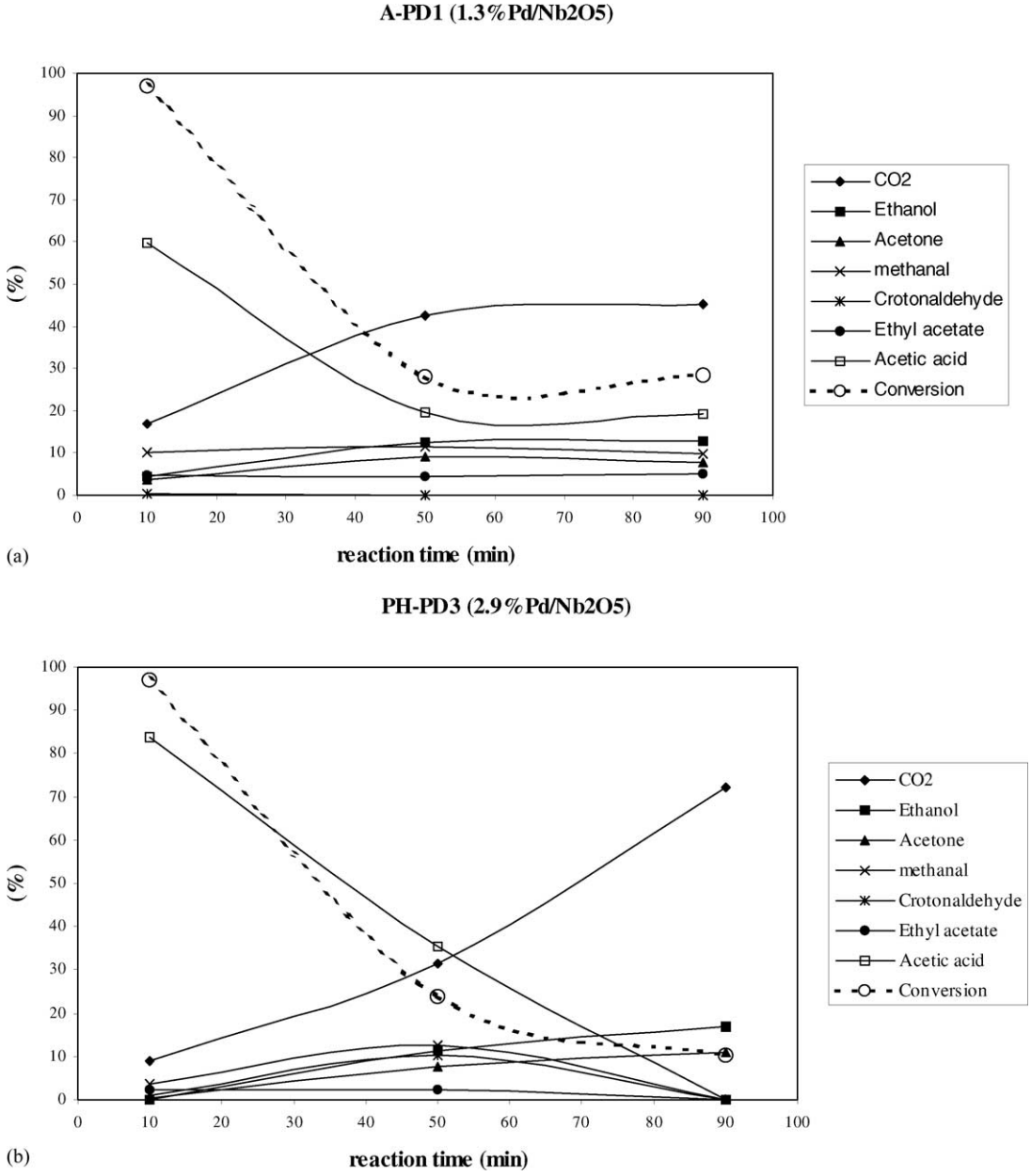

Fig. 9. Conversion (C) and fractional (S_f) selectivities versus time for monometallic catalysts: (a) A-PD1 sample; (b) PH-PD3 sample.

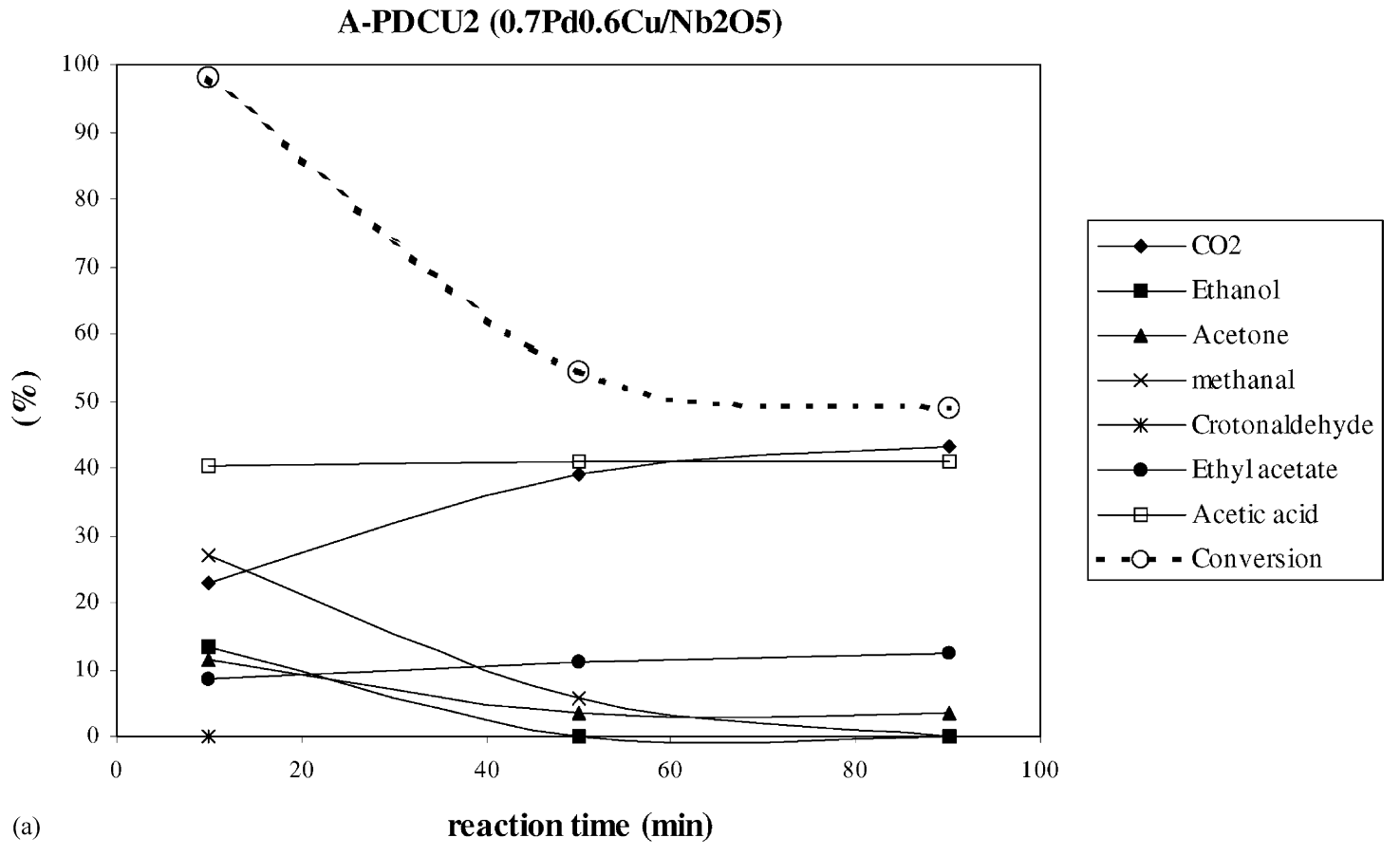

(a)

Fig. 10. Conversion (C) and fractional (S_f) selectivities versus time for bimetallic catalysts: (a) A-PDCU2 sample; (b) PH-PDCU1 sample; and (c) PH-PDAU3 sample.

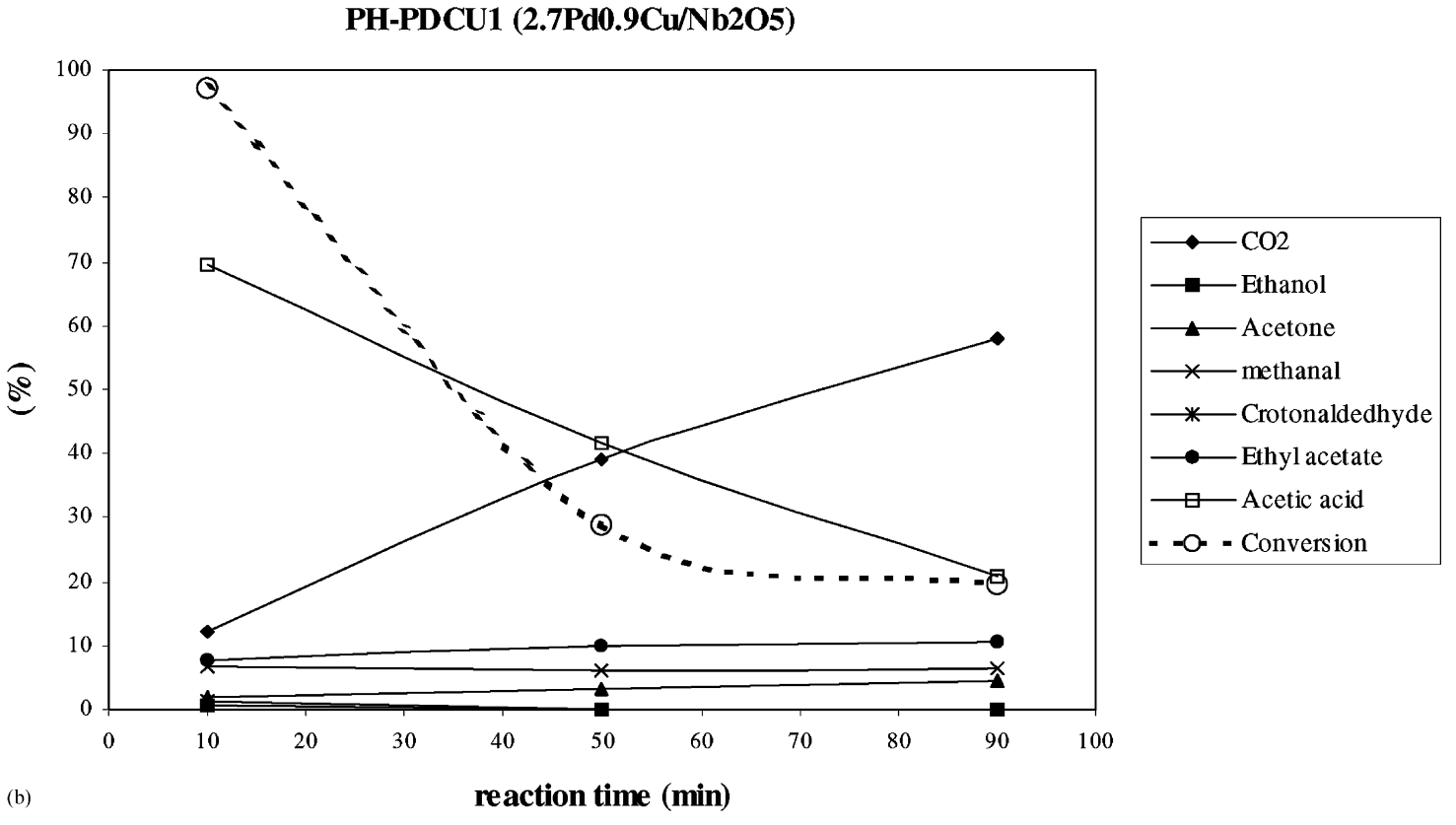

(b)

Fig. 10. (*Continued*).

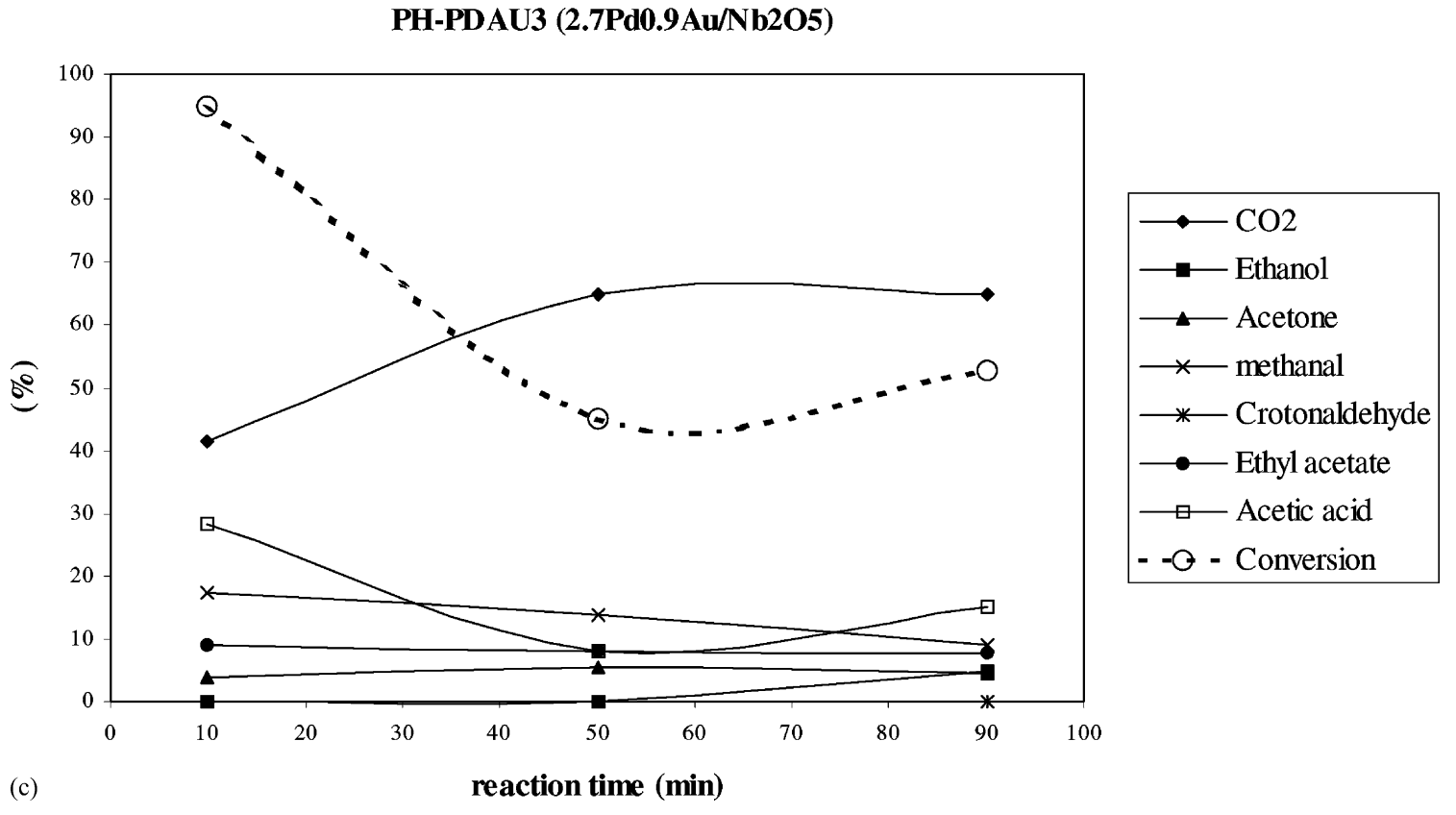

(c)

Fig. 10. (*Continued*).

Boudart [31] on Pd–Au/SiO_2, who reported also that gold addition increases 50 times the water formation rate from H_2 and O_2 [32].

3.3. Catalytic tests

All samples are subject to a marked deactivation and the performances, summarized in Table 3, are compared after 90 min; the selectivity to CO_2 (S_{CO_2}) is initially near zero and increases with time, whereas the selectivity to acetic acid, initially important, decreases in most cases (Figs. 9 and 10). The ethanal oxidation reaction mechanism is believed to be very complex [33]. During the reaction, the products are formed either by direct oxidation or from parallel reactions between the byproducts formed. The main products are CO_2, acetic acid, ethanol, acetone, methanal and H_2O (not quantified). A very small amount of crotonaldehyde was recorded on the PH-PD3 sample at 25% conversion. The formation of acetone may be ascribed to the reaction of acetic acid on niobia acid sites, as previously claimed on Cr_2O_3, Fe_2O_3 and ZrO_2–Al_2O_3 catalysts [33-36]. CO_2, acetic acid, methanal and ethanol are formed from ethanal, but ethanol is rapidly consumed by acetic acid to give ethyl acetate [6]. CO_2 is also formed from acetic acid during the reaction.

3.3.1. Palladium catalysts

Both samples show a marked deactivation; after 90 min, the conversion drops to 10% (PH-PD3) and 30% (A-PD1) of the initial values (Fig. 9). On the other hand (S_{CO_2}) increases up to 45% for A-PD1 and 72% for PH-PD3. Moreover (S_{AcOH}) strongly decreases during the reaction due to the acetic acid oxidation to CO_2.

The CO_2 production over A-PD1 is greater than over PH-PD3 (Table 1). For A-PD1, the strong catalyst deactivation was ascribed to (i) H_2O production and (ii) surface palladium oxidation, whereas for PH-PD3 the agglomeration of Pd particles is involved (observed by XRD diffraction, IR chemisorption of CO and H_2 chemisorption). According to H_2 chemisorption measurements, the MFE of PH-PD3 sample decreases from 45 to 10% after pre-treatment at 300 °C under flowing H_2/N_2.

In both cases, CO_2 is formed from oxidation of ethanal and/or acetic acid (these products disappear when the CO formation increases).

3.3.2. Bimetallic catalysts

The addition of a second metal diminish the catalyst deactivation in all cases and the influence of the preparation method is evidenced.

On the A-PDCU2 sample, the CO_2 production is higher than on A-PD1 while (S_{AcOH}) is constant during the reaction (40%) (Fig. 10a). In this case, CO_2 is formed only from oxidation of ethanal. The higher acetic acid production can be ascribed to the predominant presence of Cu^{n+} species over Pd^0–CO entities, as deduced from IR spectra of adsorbed CO (Fig. 5).

On PH-PDCU1 (S_{CO_2}) increases from 20 to 60%, while (S_{AcOH}) decreases from 70 to 20% (Fig. 10b). In this case, CO_2 is formed from oxidation of either ethanal or acetic acid, like on the PH-PD3 monometallic sample, but the deactivation is lower on the bimetallic sample. Copper addition also favors the ethyl acetate formation (∼10%) due to the reaction between ethanol and acetic acid.

The Pd–Au system behaves differently. During the reaction (S_{CO_2}), always higher than (S_{AcOH}), is comparable to the value measured on PH-PD3 but with a conversion five times higher (Fig. 10c). This behavior can be attributed to (i) an *electronic effect* (Au → Pd electron donation), which precludes the surface oxidation of palladium particles, as observed by IR spectroscopy of adsorbed CO (Fig. 8) and (ii) a Pd–Au f.c.c. alloy formation (observed by XRD; Fig. 7). Moreover, S_{AcOH} is lower than 20% during the reaction and the byproducts formed (ethanol, methanal and ethyl acetate) are also lower than 17%.

4. Conclusions

The notable deactivation observed on monometallic palladium catalysts in the oxidation of acetaldehyde is significantly attenuated by the addition of a second metal such as Cu or Au.

The preparation method has a marked influence on the catalytic performances: (i) the best performance (high CO_2 production, low AcOH formation) is obtained with the Pd–Au sample prepared by photoreduction; this peculiarity is ascribed to a Au → Pd electron donation which prevents the surface oxidation of palladium particles; (ii) conversely, preferential formation of AcOH is recorded on the Pd–Cu sample

prepared by anchoring; this behavior is credited to the predominance of Cu^{n+} species.

Finally, the CO_2 productivity values presented above are higher than those reported over heteropoly-compounds in the same conditions (about 10^{-6} mol g^{-1}) [6].

Acknowledgements

The authors are indebted to CNPq-Brazil for support and financial resources.

References

[1] (a) E.I. Ko (Ed.), Catalytic conversion with niobium materials, Catal. Today 8 (1) (1990).;
(b) K. Tanabe (Ed.), Preparation, physicochemical properties and catalytic activity of niobium materials, Catal. Today 16 (3–4) (1993).;
(c) K. Tanabe (Ed.), Catalytic properties of niobium materials and related subjects materials, Catal. Today 28 (1–2) 1996.
[2] F.B. Passos, D.A.G. Aranda, R.R. Soares, M. Schmal, Catal. Today 43 (1998) 3.
[3] (a) F.B. Noronha, A. Frydman, D.A.G. Aranda, C. Perez, R.R. Soares, B. Morawek, D. Castner, C.T. Campbell, R. Frety, M. Schmal, Catal. Today 28 (1996) 147;
(b) M.M. Pereira, F.B. Noronha, M. Schmal, Catal. Today 16 (1993) 407.
[4] R. Brayner, D. Ciuparu, F. Fievet-Vincent, G.M. Cruz, F. Bozon-Verduraz, Catal. Today 57 (2000) 261.
[5] J.J. Spivey, Ind. Eng. Chem. Res. 26 (1987) 2165.
[6] (a) N. Mizuno, T. Watanabe, H. Mori, M. Misono, J. Catal. 123 (1990) 157;
(b) H. Mori, N. Mizuno, M. Misono, J. Catal. 131 (1991) 133.
[7] R. Brayner, G. Viau, G.M. Cruz, F. Fiévet-Vincent, F. Fiévet, F. Bozon-Verduraz, Catal. Today 57 (2000) 187.
[8] J.-M. Herrmann, J. Disdier, P. Pichat, J. Catal. 113 (1988) 72.
[9] A. Bensalem, G.A. Shafeev, F. Bozon-Verduraz, Catal. Lett. 37 (1996) 63.
[10] R. Brayner, G.A. Shafeev, G. Viau, L. Gengembre, F. Bozon-Verduraz, in press.
[11] A. Fernandez, G. Munuera, A.R. Gonzalez-Elipe, J.P. Espinoz, Appl. Catal. 57 (1990) 191.
[12] A. Rakai, D. Tessier, F. Bozon-Verduraz, New J. Chem. 16 (1992) 869.
[13] R. Brayner, S. Ammar-Merah, F. Villain, F. Bozon-Verduraz, in press.
[14] N. Sheppard, T.T. Nguyen, in: R.J.H. Clark, R.E. Hester (Eds.), Advances in Infrared and Raman Spectroscopy, vol. 5, Wiley, New York, 1978, p. 67.
[15] (a) A. Ortega, A.M. Hoffman, A.M. Bradshaw, Surf. Sci. 119 (1982) 79;
(b) M.A. Chesters, G.S. McDougall, M.E. Penple, N. Sheppard, Surf. Sci. 164 (1985) 425.
[16] S. Ichikawa, H. Poppa, M. Boudart, J. Catal. 91 (1985) 1.
[17] H.A.C.M. Hendrickx, C. Des Bouvrie, V. Ponec, J. Catal. 109 (1988) 120.
[18] (a) Y.A. Bradshaw, F. Hoffman, Surf. Sci. 72 (1978) 513;
(b) A. Ortega, F.M. Hoffman, A.M. Bradshaw, Surf. Sci. 119 (1982) 79.
[19] D. Tessier, A. Rakai, F. Bozon-Verduraz, J. Chem. Soc., Faraday Trans. 88 (1992) 741.
[20] E.A. Sales, J. Jove, M.J. Mendes, F. Bozon-Verduraz, J. Catal. 195 (2000) 88.
[21] D. Amalric-Popescu, F. Bozon-Verduraz, Catal. Today 70 (2001) 139.
[22] F.B. Noronha, M. Schmal, M. Primet, R. Frety, Appl. Catal. 78 (1991) 125.
[23] A.B.P. Lever, Inorganic Electronic Spectroscopy, 2nd ed., Elsevier, Amsterdam, 1984, p. 440.
[24] F. Aubke, C. Wang, Coord. Chem. Rev. 137 (1994) 483.
[25] M.I. Bruce, J. Organometall. Chem. 44 (1972) 209.
[26] A. Davydov, IR Spectroscopy Applied to Surface Chemistry of Oxides, Nauka, Novosibirsk, 1984.
[27] P. Hollins, Surf. Sci. Rep. 16 (1992) 51.
[28] K.H. Huang, J. Mol. Catal. 64 (1991) 85.
[29] J. Pritchard, T. Catterick, R.K. Gupta, Surf. Sci. 53 (1975) 1.
[30] K.I. Hadjiivanov, M.M. Kantcheva, D.G. Klissurski, J. Chem. Soc., Faraday Trans. 92 (1996) 4595.
[31] E.L. Kugler, M. Boudart, J. Catal. 59 (1979) 201.
[32] Y.L. Lam, J. Criado, M. Boudart, Nouv. J. Chimie 1 (1977) 461.
[33] (a) J.C. Kuriacose, C. Daniel, R. Swaminathan, J. Catal. 12 (1968) 19;
(b) J.C. Kuriacose, S.S. Jewur, J. Catal. 50 (1977) 330.
[34] V.I. Yakerson, L.I. Lafer, A.L. Klyochko-Gurvich, A.M. Rubinshtein, Izv. Akad. Nauk. SSSR 83 (1966).
[35] G. Blyholder, E.A. Richardson, J. Phys. Chem. 66 (1962) 2597.
[36] R.L. Burwell, G.L. Haller, K.C. Taylor, J.C. Read, in: D.D. Eley, H. Pines, P.B. Weisz (Eds.), Advances in Catalysis, vol. 20, Academic Press, New York, 1969, p. 3.